



University
of Glasgow

Ukai, T., Zare-Behtash, H., Lo, K. H., Kontis, K., and Obayashi, S. (2014) *Effects of dual jets distance on mixing characteristics and flow path within a cavity in supersonic crossflow*. International Journal of Heat and Fluid Flow, 50 . pp. 254-262. ISSN 0142-727X

Copyright © 2014 Elsevier Inc.

A copy can be downloaded for personal non-commercial research or study, without prior permission or charge

Content must not be changed in any way or reproduced in any format or medium without the formal permission of the copyright holder(s)

When referring to this work, full bibliographic details must be given

<http://eprints.gla.ac.uk/99579/>

Deposited on: 01 December 2014

Enlighten – Research publications by members of the University of Glasgow
<http://eprints.gla.ac.uk>

Effects of dual jets distance on mixing characteristics and flow path within a cavity in supersonic crossflow

Takahiro Ukai^{1*}, Hossein Zare-Behtash², Kin Hing Lo², Konstantinos Kontis², Shigeru Obayashi¹

¹*Institute of Fluid Science, Tohoku University, 2-1-1 Katahira, Aoba-ku, Sendai, Miyagi, 980-8577, Japan*

²*School of Engineering, University of Glasgow, Scotland G12 8QQ, UK*

***Corresponding author: Takahiro Ukai**

Email: ukai@edge.ifs.tohoku.ac.jp

Telephone/Fax: + 81-22-217-5257

Abstract:

A rectangular open cavity with upstream dual injectors at a freestream Mach number of 1.9 was investigated experimentally. To evaluate the effect of the distance between the jets, the flow characteristics were investigated using the high-speed schlieren photography, particle image velocimetry, and surface oil flow techniques. The dual jet distances of 18 and 54 mm were used. Unstable flow occurs over the cavity in all cases and is not improved by changing the distance between the dual jets. Although the distance between the dual jets does not influence the flow stability, the flow field varies decidedly depending on the dual jets distance. The enhancement of air mixing depends on the distance between the jets. A long dual jets distance was found to yield better mixing characteristics within the cavity than a short one. When the jets are further apart, the mainstream between two counter-rotating vortex pairs behind the jets flows strongly into the cavity because of the increased blow-down occurring between the vortex pairs. Additionally, a counterflow with a low velocity magnitude occurs behind the jets. Hence, mixing is enhanced within the cavity by effects of the opposed flow. When the jet pairs are closer to each other, the counter-rotating vortex pairs are in contact; as a result, the blow-down effect does not occur between them. The flow drawn into the cavity from the mainstream is supplied from the sides of the test section into the cavity.

Keywords:

Mixing characteristics, Flow path, Supersonic dual injections, Cavity, Scramjet

1. Introduction

Supersonic combustion ramjet (scramjet) engines require an optimized injection system that produces higher performance due to enhanced fuel-air mixing and improved flame stabilization. Additionally, a low profile drag is a key component that will increase the net power. Designing the optimum injection system having all of these capabilities is challenging. Because a scramjet engine is mounted on hypersonic vehicles working at Mach numbers ranging from 4 to 8 [1], the residence time of the supersonic freestream within the combustion chamber of a scramjet is extremely short, typically on the order of milliseconds. It is not easy to design the optimum injector because of the high-speed flow and short residence time.

Having a flush-mounted multiple injection system is an effective means of combining the benefits of low profile drag injection with improved mixing characteristics. Flush-mounted multiple injection systems have been shown to enhance the fuel-air mixing characteristics [2-4]. Pudsey and Boyce [5] has shown that the multiport jet arrays are more effective for mixing in the near field around the injection location, although the mixing is not improved in the far field compared to that in a single injection system. Ming-bo et al. [6] investigated the effect of the distance between the injection ports on the mixing characteristics in a parallel multiple injection model. When the distance between the multiple ports in parallel injection is short, an adequate the mainstream is not supplied between them, and the mixing effect is decreased. This is because of the interaction between the bow shocks in front of the injected jets. To obtain optimum mixing characteristics, it is necessary to investigate the mixing phenomena in a simplified multiple injection model. In multiple injection systems, a complex flow field behind the injectors is induced by many shock wave interactions generated around the multiple injections, making it difficult to fully understand the mixing characteristics. For a tandem dual injection system, Lee [2] has shown that the mixing characteristics of the dual injection system are enhanced compared to those of a single injection system. A rear injection flow possesses higher penetration and diffusion because the mainstream is blocked in front injection. An optimal distance between the front and rear jets exists at which better mixing is obtained.

A cavity model enhances the fuel-air mixing and flame holding properties of scramjet engines [7-17]. Yu et al. [18] has shown that a cavity model can induce faster mixing and a high combustion pressure, although the combustion performance depends on the cavity configuration. Cavity models are classified as open cavity or closed cavity depending on the cavity geometry: length-to-depth ratio (L/D). In general, an open cavity ($L/D < 7-10$) is often used as a flame stabilizer because of its low drag properties compared to a closed cavity ($L/D < 10-13$). The surface pressure on the aft wall of the closed cavity increases because the shear layer over the cavity impinges strongly on the aft wall

[19]. Although high drag also occurs in cavities with an aft ramp, even if the cavity geometry is an open one, such cavities exhibit high performance as a flame holder [9].

Although an open cavity enhances the flame stabilization and fuel-air mixing, this performance decreases if unstable flow occurs over the cavity. The shear layer usually impinges on the rear edge of the cavity and generates an acoustic wave. When pressure oscillations occur inside the cavity by the successive compression waves, the flow becomes unsteady over the cavity [20, 21]. Although stable flow can be obtained around a cavity when an aft ramp is adopted, the profile drag increases [19]. A shock-jet impingement system could be effective for unstable flow over the cavity. If a shock wave impinges on the shear layer near the rear edge of the cavity, the flow over the cavity might become steady because the shear layer is lifted up by the shock interaction [10].

The mixing and flame holding capability varies depending on the injector position. For open cavities containing a fuel injector within the cavity, the presence of an aft ramp provides high performance as a flame holder, although the performance varies with the injector position [9, 15]. Even for a cavity with an upstream injector and a straight aft wall, which possesses lower drag than a cavity with an aft ramp, the mixing characteristics depend on the injector position. Ukai et al. [22] have shown that if an injector is positioned farther from the cavity front edge, the mixing is decreased. For an injection position close to the cavity, the mixing is enhanced within the cavity, and stable mixing performance can be obtained independent of the jet-to-free stream momentum flux ratio.

It is necessary to design an optimum injection system for the development of scramjet engines. The cavity model exhibits higher fuel-air mixing and flame stabilization performance, although these characteristics depend on the cavity configuration and injector position. Additionally, a flush-mounted multiple injection system can enhance the mixing. An open cavity with a flush-mounted multiple injection system could be the solution for higher combustion performance. However, it is difficult to accurately understand the flow field around a cavity with multiple injection ports because many shock interactions occur around the injections. In this study, to understand the flow physics around a cavity with injections, in particular the air mixing and flow stability, an experimental investigation was performed in a wind tunnel at a Mach number of 1.9. To simplify the study, a dual injector with a rectangular open cavity was adopted. The dual jets distance was varied, and the flow field was investigated using the high-speed schlieren photography, particle image velocimetry (PIV), and surface oil flow techniques.

2. Experimental setup

2.1 Experimental conditions

The experimental investigation was performed at a Mach number of 1.9 in the Aero-Physics Laboratory trisonic wind tunnel at The University of Manchester [22]. A schematic diagram of the cavity geometry is shown in Fig. 1. A rectangular open cavity with $L/D = 5$ [100 mm in length (L) and 20 mm in depth (D)] was adopted and embedded into the lower wall of the test section. A converging round jet orifice with an exit diameter of 2.2 mm was vertically machined upstream of the cavity. The jet orifices were located 10 mm from the front edge of the cavity. Ukai et al. [22] showed that the air mixing is enhanced within the rectangular open cavity with $L/D = 5$ when the jet is positioned 10 mm from the front edge of the cavity. The distance between the dual jets was $3BL$ (18 mm, Case 1) or $9BL$ (54 mm, Case 2), where BL is the boundary layer thickness at the jet hole location. A test case with no jet (Case 0) was also considered.

Different distances between the jet injections were used to investigate the flow physics, especially the flow mixing characteristic, flow stability, and flow pattern within the cavity. High-pressure air supplied through a pressure regulator and flexible tubing was used as the jet gas. Flexible tubes separated from the outlet of a pressure regulator supplied high pressure air for each jet. Only one pair of jet holes was operated at a time, either the jets that are $3BL$ apart or the pair that is $9BL$ apart. The jet pressure was adjusted to provide a jet-to-free stream momentum flux ratio of $J = 5.3$; J is defined as Eqn. 1,

$$J = \frac{\gamma_{jet} p_{jet} M_{jet}^2}{\gamma_0 p_0 M_0^2} \quad (1)$$

where γ is the specific heat ratio, p is the static pressure, and M is the Mach number, and subscripts “0” and “jet” refer to the freestream and jet conditions, respectively.

2.2 High-speed schlieren photography

High-speed schlieren photography [23-26] with a standard Z-type optical arrangement was employed to visualize the flow field around the cavity. The optical arrangement consists of a pair of 203.3 mm diameter parabolic mirrors with 1016 mm in focal length and a 450 W Xenon continuous light source (Newport). The light generated from the light source is cut off by a slit and collimated by a parabolic mirror. The collimated light passes through the test section and is reflected by the second parabolic mirror. The offset angle between the collimated light beam and the light source was set to 10° to prevent coma. A knife edge is located at the focal point of the second mirror to adjust the sensitivity. High-speed schlieren images were recorded using a high-speed video camera (Fastcam SA-1, Photron Corp.) with a maximum resolution of 1024×1024 pixels. A frame rate of 8.0 kfps

with an exposure time of 1 μs was used.

2.3 Particle image velocimetry

PIV was used to evaluate the flow velocity and other properties inside the cavity. The PIV system has been successfully applied in previous studies [27-29]. A Nd:YAG Q-switched laser (Litron Nano PIV series, LPU550) having a pulse energy of 200 mJ at a repetition rate of 15 Hz and wavelength of 532 nm with a pulse duration of 4 ns was used for the PIV illumination. A laser illuminator was located at the side of the test section, and a planar laser sheet was illuminated parallel to the front edge of the cavity. The laser beam was pulsed at intervals of $\Delta t = 0.9 \mu\text{s}$ between two consecutive images to obtain sufficient displacement of the tracer particles suitable for the current velocity range of 500 m/s.

Olive oil particles with 1 μm in diameter were produced using TSI's Oil Droplet Generator (model 9307-6), with an aerosol flow rate of 1000 L/min. To provide adequate and uniform seeding inside the cavity, particles were introduced at the inlet of the wind tunnel, and continuous seeding was provided during the tunnel run time. A suitable seeding particle diameter and density are required to capture the flow tracing accurately [30]. Ukai et al. [22] showed that the velocity field can be captured accurately using olive oil particles with 1 μm in diameter.

A double-frame high resolution CCD camera (LaVision Imager Pro X 2M) with 1600×1200 pixels resolution was used to record the light scattered by the particles. The camera records images at 14-bit digitization. The camera, equipped with a band-pass filter of $532 \pm 5 \text{ nm}$, viewed the laser sheet orthogonally. The recorded images were initially divided into 32×32 pixel interrogation windows and then processed with a cross-correlation algorithm using the DaVis 7.2 software. The interrogation windows were refined to 16×16 pixel squares. A 50% overlap was employed to improve the spatial resolution and prevent the appearance of spurious vectors by adaptively improving the window size [31]. A data set of 60 instantaneous vector fields was acquired during 6 s of the wind tunnel running time. Because it takes some time to establish an uniform flow in the wind tunnel and also particles run out after a few seconds, the averaged velocity field was calculated by the DaVis software from a total of usable 40 image pairs; the time intervals used to determine the averaged velocity were 4 seconds long.

2.4 Fluorescent oil flow

The oil flow recipe was optimized for the current experimental conditions. This ensured that the oil does not dry too quickly, allowing sufficient time for the flow to become established, but at the same time it is not so viscous that it does not follow the flow streamlines and obstructs the flow.

The formulation used a fluorescent powder suspended in paraffin, oleic acid, and silica gel as the oil material. The oil was poured inside the cavity near the aft wall and illuminated by UV LEDs with a peak wavelength of 395 nm. The LED panels were located on both sides of the test section to provide uniform lighting. Images were recorded using a SLR camera (Canon, EOS-450D) with 12 Mpixels resolution, positioned above the test section. The camera is set to continuous shooting mode at 3.5 fps, and the shutter speed was set at a minimum of 0.25 ms.

3. Results and discussion

3.1 Density field

Figure 2 shows instantaneous high-speed schlieren images of the density field around the cavity for all the cases. Although a gap shock was produced from the gap between the supersonic insert and the straight section of the wind tunnel upper wall, it does not affect the results because it was weak. The some flow characteristics are similar to the results of Ukai et al. [22], however, different flow fields were observed depending on the dual jets distance. Flow field schematics of the cavity with the dual jets in Cases 1 (18 mm apart) and 2 (54 mm apart) are shown in Fig. 3. The angle of the bow shock in front of the jets in Case 1 was larger than that in Case 2. This is because the bow shocks at each jet interfere if the distance between the dual jets is short [6]. Additionally, because the bow shocks in front of the jets did not interact strongly with one another in Case 2, an impinging bow shock appeared between the jet holes.

Unstable flow appeared over the cavity in all cases even when air was jetted from the dual injectors. Acoustic waves were continuously present over the cavity. They originated from the impact between the shear layer and the aft wall of the cavity. Since the shear layer became attached to the aft wall of the cavity in all cases, the flow became unstable over the cavity. In Cases 1 and 2, although the air mixing might be enhanced by the turbulent shear layer, an unstable flow condition appeared over the cavity.

The separation shock from the front edge of the cavity oscillated in the dual jet cases, and its oscillatory intensity differed between Cases 1 and 2. Ukai et al. [22] showed that the oscillating separation shock is generated by interaction of the separation shock with a compression shock generated behind the jet. In the present results, the largest amplitude appeared in Case 2, although the oscillation occurred in both cases. In Case 1, the compression shocks behind each jet might interact because the distance between the dual jets is short; as a result, the compression shocks may become weak. On the other hand, in Case 2 with a longer distance between the dual jets, the compression shock behind each jet is not affected by its counterpart; therefore, the compression shocks interact strongly with the separation shock.

3.2 Flow structure

The vorticity component along the Z direction in the plane 10 mm above the cavity floor, calculated on the basis of the PIV data, is shown in Fig. 4. The horizontal and vertical axes indicate the cavity width and length, respectively. The main flow direction is from top to bottom. The air mixing characteristics vary depending on the dual jets distance. In Cases 0 (no jet) and 1 (dual jets 18 mm apart), the vorticity distribution was almost identical within the entire cavity area, although a slight difference in vorticity was observed because of the jet interaction at the fore wall of the cavity in Case 1. On the other hand, in Case 2 (dual jets 54 mm apart), distinct vortex structures appeared near the aft wall of the cavity. The air mixing is enhanced within the cavity because negative and positive vorticity appear adjacent to one another. The vorticity component in the Z direction is an important factor for the air mixing because mixing over a large region within the cavity is beneficial; of course, the mixing by the vorticity component along the X direction is also important. Table 1 shows the averaged root-mean-square flow velocity along the cavity centerline (approximately $X = 55$ mm). $V_{x\ rms}$ and $V_{y\ rms}$ are the averaged root-mean-square velocities in the X and Y directions, respectively. Although $V_{x\ rms}$ and $V_{y\ rms}$ became larger in Case 2 than in Case 1, a large difference in $V_{x\ rms}$ between Cases 1 and 2 did not appear. Figure 5 shows the root-mean-square velocity contours in the Y direction. The turbulence intensity is stronger in Case 2 than in the other cases, and strong turbulence intensity is widely distributed, enhancing the mixing. This means that the air mixing is not necessarily enhanced within the cavity with the introduction of the dual jets upstream, and there is a strong dependence on the injection location.

To investigate the cause of the mixing enhancement, the velocity field in the plane of the cavity was visualized by PIV measurements. Figures 6, 7, and 8 show the averaged velocity in the planes 30, 20, and 10 mm above the cavity floor, respectively. The contour shows the velocity magnitude in the X and Y directions.

Because opposed flow within the cavity occurs, remarkable mixing characteristics can be obtained. The flow direction was the same in all the cases in the plane 30 mm above the cavity floor (Fig. 6), although the velocity decreased behind the jets because of the jet boundary. The velocity distribution in Case 0 (no jet) is not shown since the velocity did not change. The effect of the dual jets distance did not produce any difference in the flow pattern between Cases 1 and 2. In the plane 20 mm above the cavity floor (Fig. 7), a counterflow and low velocity magnitude appeared behind the jets in Cases 1 and 2. The flow direction at the low velocity magnitude changed at the aft wall. It is conjectured that it flowed into the cavity because the shear layer was expanded by jet interaction. In Case 0, the flow direction became the same as the mainstream, although a low velocity magnitude occurred on

the cavity centerline. This is because the flow was supplied from inside the cavity to the fore wall of the cavity on the cavity centerline. In the plane 10 mm above the cavity floor (Fig. 8), the counterflow was maintained behind the jets in Cases 1 and 2. In Case 2, opposed flow was generated within the cavity, enhancing the mixing within the cavity. On the other hand, in Case 1, effective mixing characteristics cannot be obtained, contrast to Case 2, because the flow pattern resembled that in Case 0. However, the jet flow still influences the flow field within the cavity because the velocity magnitude was more complicated than that in Case 0.

The oil flow patterns on the cavity floor are shown in Fig. 9. The flow path was obtained from images separated by time intervals of 0.25 ms. Figure 10 shows three-dimensional flow field schematics of the cavity. A counter-rotating vortex pair generally appears behind a jet in the jet boundary, and its boundary grows with increasing downstream distance [32].

Although the mainstream was drawn into the cavity, the flow path in Case 1 differed from that in Case 2. In Case 2, the flow separation line did not appear near the fore wall of the cavity on the cavity centerline because the mainstream passes through the area between the jets, and the counter-rotating vortex pairs behind the jets supply the mainstream to the cavity [Fig. 10 (b)]. Additionally, the inflow volume might be larger than that in Case 1. The mainstream between two counter-rotating vortex pairs flows strongly into the cavity because of the increased blow-down occurring between the vortex pairs. In Case 1, the flow drawn into the cavity from the mainstream is supplied from the sides of the test section into the cavity [Fig. 9 (b)]. The two counter-rotating vortex pairs interact, and blow-down does not occur between the pairs [Fig. 10 (a)]. Figure 11 shows the velocity profiles along the Y direction in the plane 30 mm above the cavity floor; the interaction of the counter-rotating vortex pair behind the jets can be confirmed by the differing velocity profile at 10, 40, and 80 mm from the rear edge of the cavity. The velocity behind the jets is decreased by blockage effects on the mainstream. In Case 1, at 10 mm from the rear edge of the cavity, the flow occurring behind the jets at low velocity magnitude grew with increasing downstream distance, and it was combined [Fig. 11(c)] because the jet distance was short. Figure 12 shows the Y direction flow velocity profile along the cavity centerline in the plane 20 mm above the cavity floor. Negative velocity appeared on the cavity centerline in Case 1, and instead of the mainstream with positive velocity, negative velocity appeared on the cavity centerline. Hence, the mainstream cannot flow into the cavity from between the jets because two counter-rotating vortex pairs interact. On the other hand, for Case 2, the two peaks at low velocity did not combine in the plane 30 mm above the cavity floor (Fig. 11). In the plane 20 mm above the cavity floor (Fig. 12), the mainstream with positive velocity is supplied from between the jets to the cavity along the cavity centerline.

4. Conclusion

An experimental investigation was performed to understand the mixing and flow stability characteristics inside a rectangular open cavity with upstream dual injectors at a freestream Mach number of 1.9. The effect of the dual jets distance on the flow physics was investigated using the high-speed schlieren photography, PIV, and surface oil flow techniques. Distances between the dual jets of 18 and 54 mm were examined.

Unstable flow occurred over the cavity in all cases, and it was not improved even by varying the dual jets distance. Although the distance between the jets did not influence the flow stability, the flow field varied distinctly depending on the distance between the dual jets. The air mixing enhancement depended on the distance between the dual jets. When the jets were further apart, the mainstream between two counter-rotating vortex pairs behind the jets flowed strongly into the cavity because of the increased blow-down occurring between the vortex pairs. Additionally, a counterflow at low velocity magnitude occurred behind the jets. Hence, mixing was enhanced within the cavity by the effects of opposing flow. When the jets were placed close to each other, the counter-rotating vortex pairs were in contact; as a result, the blow-down effect did not occur between them. The flow drawn into the cavity from the mainstream was supplied from the sides of the test section into the cavity. In other words, because a distinct flow pattern appeared within the cavity in these cases, the mixing characteristics varied. It was found that the long dual jets distance is better than short one for the mixing characteristic within the cavity.

Although the effect of the dual jets distance is a key consideration in the design of an optimal injection system, the unstable flow condition over the cavity has to be improved for rectangular open cavities with upstream flush-mounted multiple injection systems. If the unstable flow can be improved using a shock impingement techniques or a cavity with an aft ramp, this system must be effective for the development of scramjet engines.

Acknowledgment

The first author was supported by the Tohoku University Global COE Program for cooperative research with the laboratory under Professor K. Kontis. The authors are indebted to the technical and administrative staff of the School of MACE at The Manchester University, especially to Mr. Lee Paul for the manufacture of the models.

References

1. Drummond, J.P., Bouchez, M., McClinton, C.R., 2006. Overview of NATO background on scramjet technology. NASA Techdoc 20060020216.
2. Lee, S.-H., 2006. Characteristics of dual transverse injection in scramjet combustor, Part 1: Mixing. *J. Propul. Power* 22(5), 1012-1019.
3. Jacobsen, L.S., Schetz, J.A., Ng, W.F., 2000. Flowfield near a multiport injector array in a supersonic flow. *J. Propul. Power* 16(2), 216-226.
4. Cox-Stouffer, S.K., Gruber, M.R., 1999. Effects of injector yaw on mixing characteristics of aerodynamic ramp injectors. AIAA Paper 99-0086.
5. Pudsey, A.S., Boyce, R.R. 2010. Numerical investigation of transverse jets through multiport injector arrays in a supersonic crossflow. *J. Propul. Power* 26(6), 1225-1236.
6. Ming-bo, S., Jing, L., Hai-yan, W., Jian-han, L., Wei-dong, L., Zhen-guo, W., 2011. Flow patterns and mixing characteristics of gaseous fuel multiple injections in a non-reacting supersonic combustor. *Heat Mass Transfer* 47, 1499-1516.
7. Yang, I., Lee, Y.J., Lee, K.J., Park, C., 2013. Effect of combustor configuration on flow and combustion in a scramjet engine. *J. Propul. Power* 29(3), 751-755.
8. Yu, K., Wilson, K.J., Smith, R.A., Schadow, K.C., 1998. Experimental investigation on dual-purpose cavity in supersonic reacting flows. AIAA Paper 98-0723.
9. Gruber, M.R., Donbar, J.M., Carter, C.D., Hsu, K.-Y., 2004. Mixing and combustion studies using cavity-based flameholders in a supersonic flow. *J. Propul. Power* 20(5), 769-778.
10. Sakamoto, K., Matsunaga, K., Fujii, K., Tamura, Y., 1995. Experimental investigation of supersonic internal cavity flows. AIAA Paper 95-2213.
11. Kang, S.H., Lee, J.Y., Yang, S.S., Choi, B., 2012. Effects of flameholder configurations on combustion in scramjet engines. *J. Propul. Power* 28(4), 739-746.
12. Yeom, H.W., Seo, B.G., Sung, H.G., 2013. Numerical analysis of scramjet engine with intake sidewalls and cavity flameholder. *AIAA journal* 51(7), 1566-1575.
13. Ghodke, C.D., Pranatharthikaran, J., Retaureau, G.J., Menon, S., 2011. Numerical and experimental studies of flame stability in a cavity stabilized hydrocarbon-fueled scramjet. AIAA Paper 2011-2365.
14. Tatman, B.J., Rockwell, R.D., Goynes, C.P., McDaniel, J.C., Donohue, J.M., 2013. Experimental study of vitiation effects on flameholding in a cavity flameholder. *J. Propul. Power* 29(2), 417-423.
15. Rasmussen, C.C., Driscoll, J.F., Carter, C.D., Hsu K.-Y., 2005. Characteristics of cavity-stabilized flames in a supersonic flow. *J. Propul. Power* 21(4), 765-768.

16. Lada, C., Kontis, K., 2010. Experimental studies on transitional and closed cavity configurations including flow control. *J. Aircraft* 47(2), 723-730.
17. Lada, C., Kontis, K., 2011. Experimental studies of open cavity configurations at transonic speeds with flow control. *J. Aircraft* 48(2), 719-724.
18. Yu, K.H., Wilson, K.J., Schadow, K.C., 2001. Effect of flame-holding cavities on supersonic-combustion performance. *J. Propul. Power* 17(6), 1287-1295.
19. Gruber, M.R., Baurle, R.A., Mathur, T., Hsu, K.-Y., 2001. Fundamental studies of cavity-based flameholder concepts for supersonic combustors. *J. Propul. Power* 17, 146-153.
20. Lawson, S.J., Barakos, G.N., 2011. Review of numerical simulations for high-speed, turbulent cavity flows. *Progress in Aerospace Sciences* 47, 186-216.
21. Li, W., Nonomura, T., Oyama, A., Fujii, K., 2013. Feedback mechanism in supersonic laminar cavity flows. *AIAA Journal* 51 (1) 253-257.
22. Ukai, T., Zare-Behtash, H., Erdem, E., Lo, K.H., Kontis, K., 2014. Effectiveness of jet location on mixing characteristics inside a cavity in supersonic flow. *Exp. Therm. Fluid Sci.* 54, 59-67.
23. Kontis, K., An, R., Zare-Behtash, H., Kounadis, D., 2008. Head-on collision of shock wave induced vortices with solid and perforated walls. *Phys. Fluids* 20, 1-17.
24. Zare-Behtash, H., Gongora-Orozco, N., Kontis, K., 2011. Effect of primary jet geometry on ejector performance: A cold-flow investigation. *Int. J. Heat Fluid Flow* 32, 596-607.
25. Erfani, R., Zare-Behtash, H., Kontis, K., 2012. Influence of shock wave propagation on dielectric barrier discharge plasma actuator performance. *J. Phys. D: Appl. Phys.* 45, 225201.
26. Kontis, K., Lada, C., Zare-Behtash, H., 2008. Effect of dimples on glancing shock wave turbulent boundary layer interactions. *Shock Waves* 17(5), 323-335.
27. Erdem, E., Saravanan, S., Lin, J., Kontis, K., 2012. Experimental investigation of transverse injection flowfield at Mach 5 and the influence of impinging shock wave. *AIAA Paper* 2012-5800.
28. Erfani, R., Zare-Behtash, H., Kontis, K., 2012. Plasma actuator: influence of dielectric surface temperature. *Exp. Therm. Fluid Sci.* 42, 258-264.
29. Zare-Behtash, H., Kontis, K., Gongora-Orozco, N., 2008. Experimental investigations of compressible vortex loops. *Phys. Fluids* 20, 126105.
30. Melling, A., 1997. Tracer particles and seeding for particle image velocimetry. *Meas. Sci. Technol.* 8, 1406-1416.
31. Erdem, E., Saravanan, S., Kontis, K., 2012. Air, carbon dioxide and helium transverse sonic jets in Mach 5 cross flow. 9th International ERCOFTAC Symposium on Engineering Turbulence Modelling and Measurements.

32. Gruber, M.R., Nejad, A.S., Chen, T.H., Dutton, J.C., 1995. Mixing and penetration studies of sonic jets in a Mach 2 freestream. *J. Propul. Power* 11, 315-323.

Figures

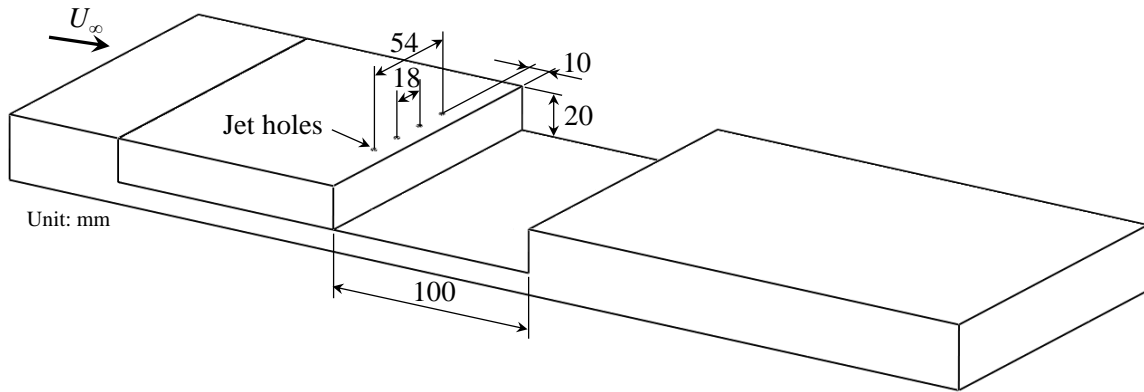
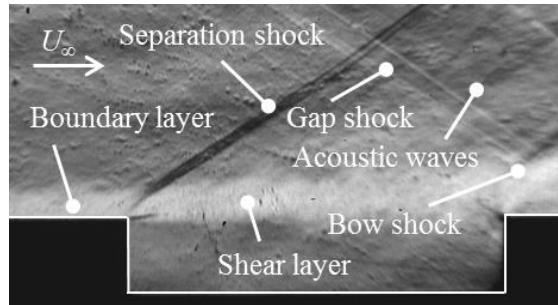
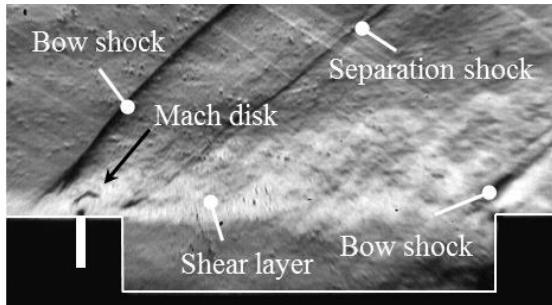


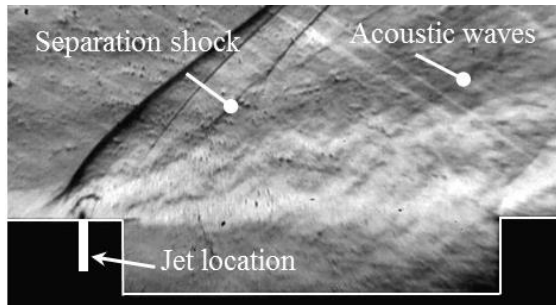
Figure 1: Cavity geometry.



(a) Case 0 (No jet)

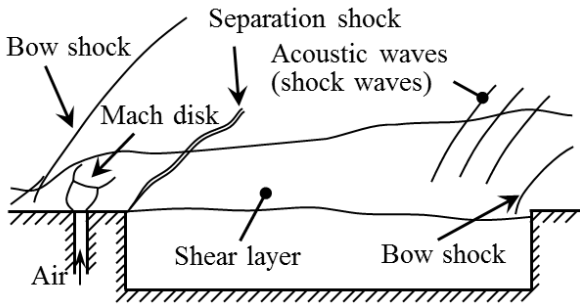


(b) Case 1 (3BL)

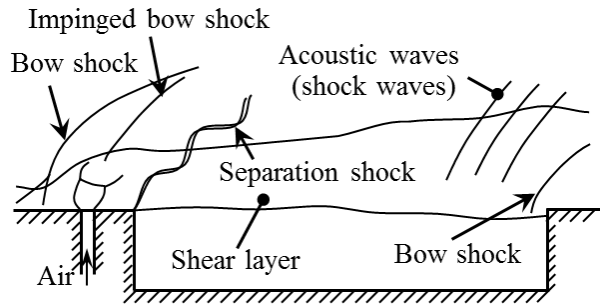


(c) Case 2 (9BL)

Figure 2: Instantaneous high-speed schlieren images.

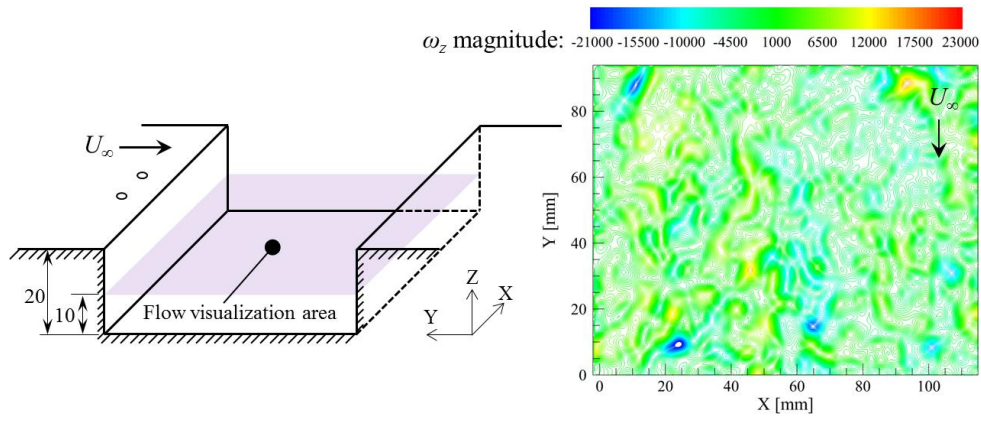


(a) Case 1 (3BL)

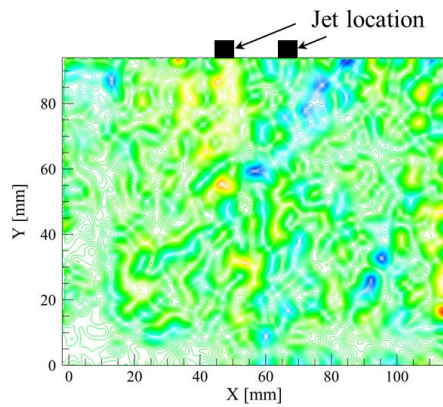


(b) Case 2 (9BL)

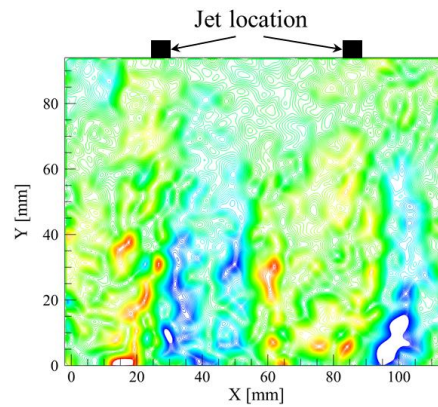
Figure 3: Flow field schematics of cavity with the dual jet distances of 3BL and 9BL.



(a) Case 0 (No jet)

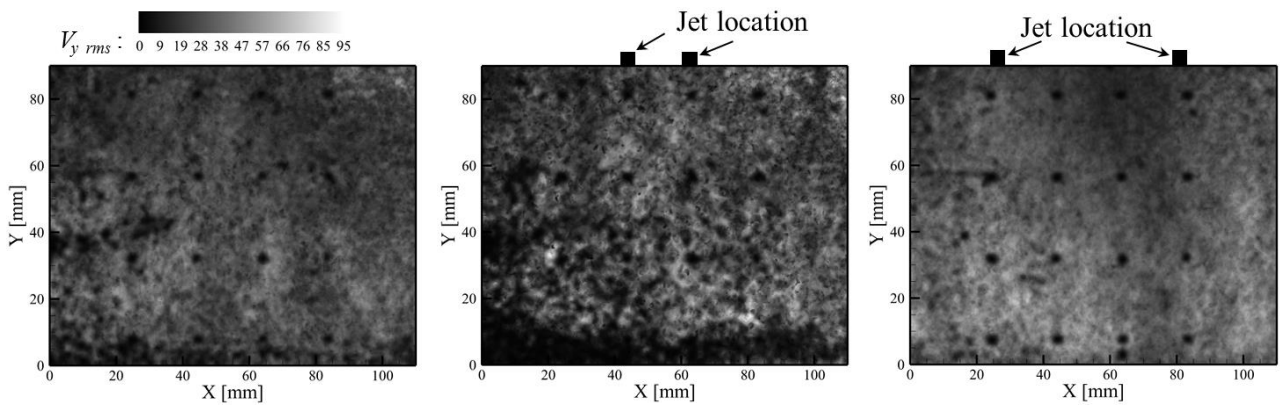


(b) Case 1 (3BL)



(c) Case 2 (9BL)

Figure 4: Vorticity component along the Z direction in the plane 10 mm above the cavity floor.



(a) Case 0 (No jet)

(b) Case 1 (3BL)

(c) Case 2 (9BL)

Figure 5: Root-mean-square flow velocity contours in the Y direction in the plane 10 mm above the cavity floor.

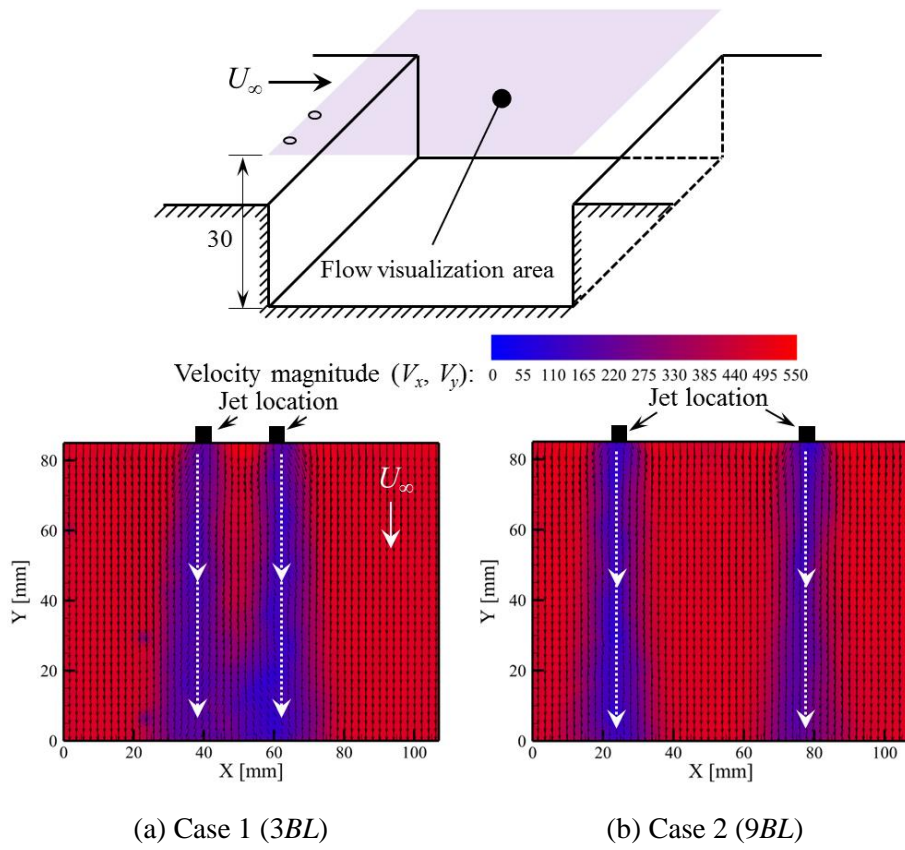
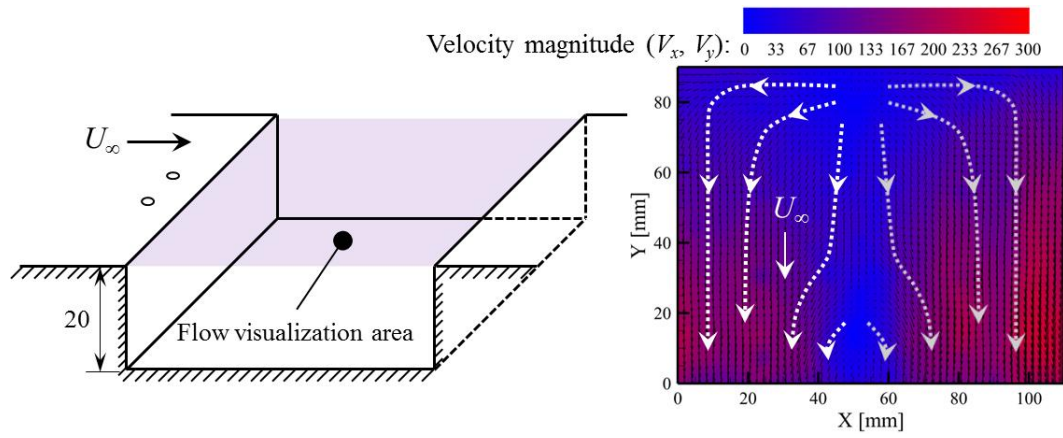
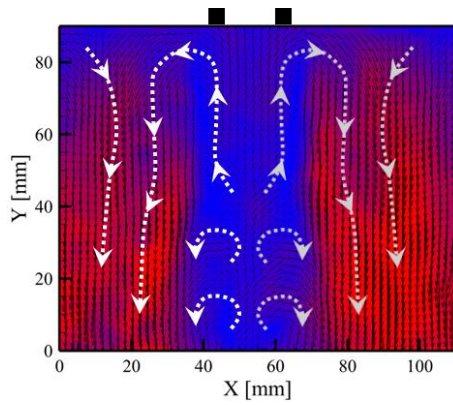


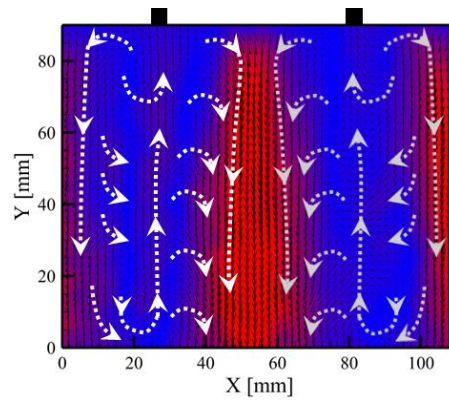
Figure 6: Averaged velocity in the plane 30 mm above the cavity floor.



(a) Case 0 (No jet)

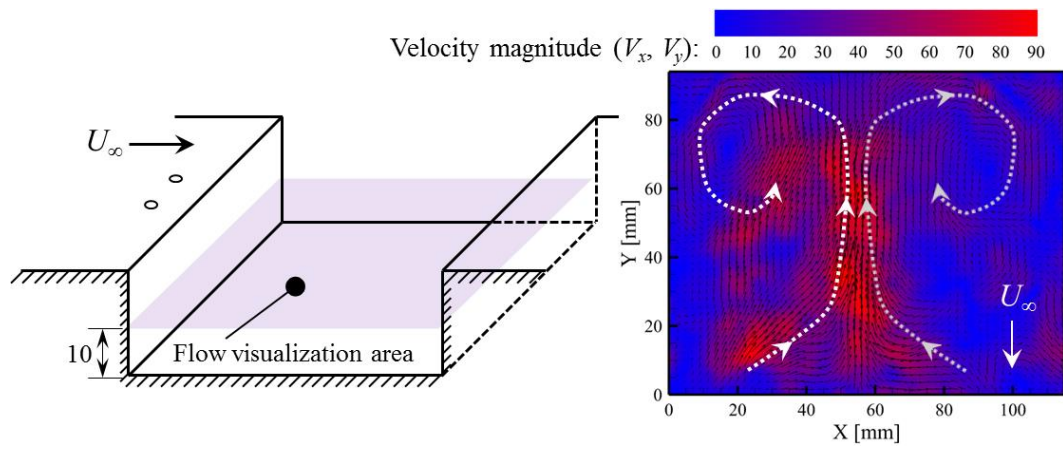


(b) Case 1 (3BL)

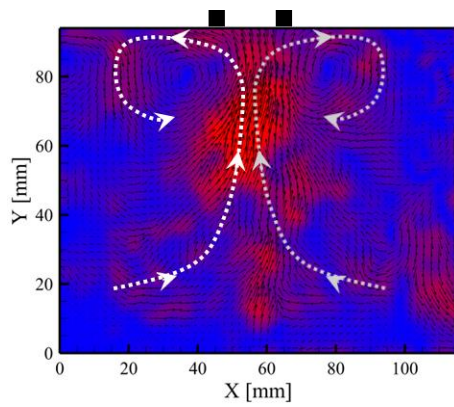


(c) Case 2 (9BL)

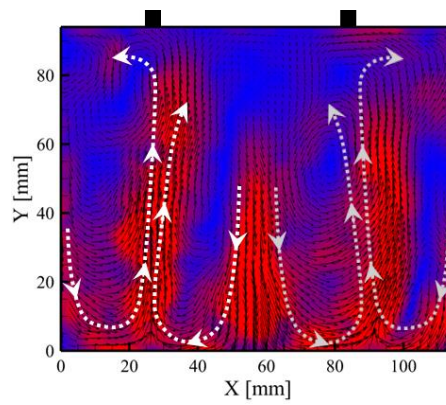
Figure 7: Averaged velocity in the plane 20 mm above the cavity floor.



(a) Case 0 (No jet)

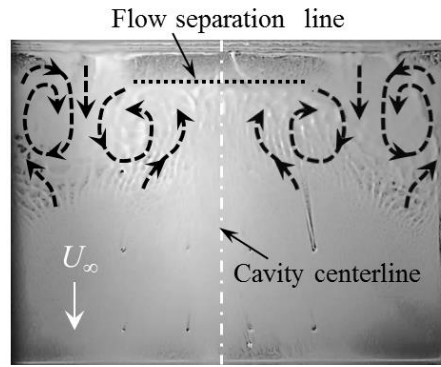


(b) Case 1 ($3BL$)

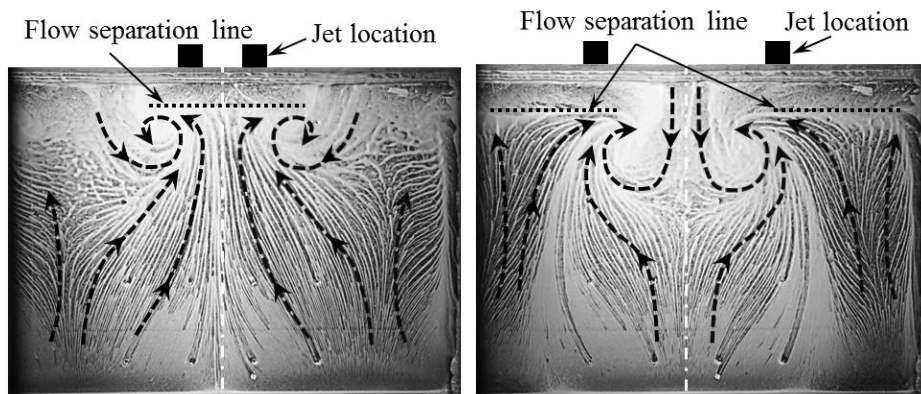


(c) Case 2 ($9BL$)

Figure 8: Averaged velocity in the plane 10 mm above the cavity floor.



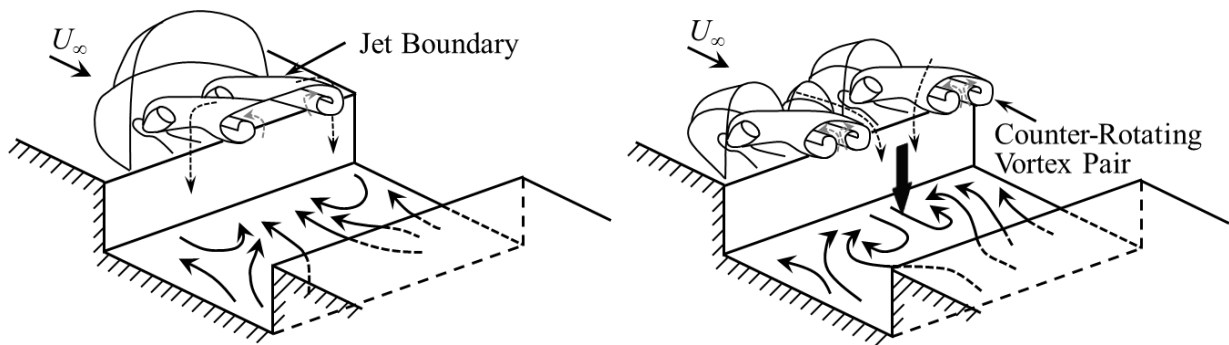
(a) Case 0 (No jet)



(b) Case 1 ($3BL$)

(c) Case 2 ($9BL$)

Figure 9: Surface oil flow visualization on the cavity floor.



(a) Case 1 ($3BL$)

(b) Case 2 ($9BL$)

Figure 10: Three-dimensional flow field schematics of the cavity with the dual jet distances of $3BL$ and $9BL$.

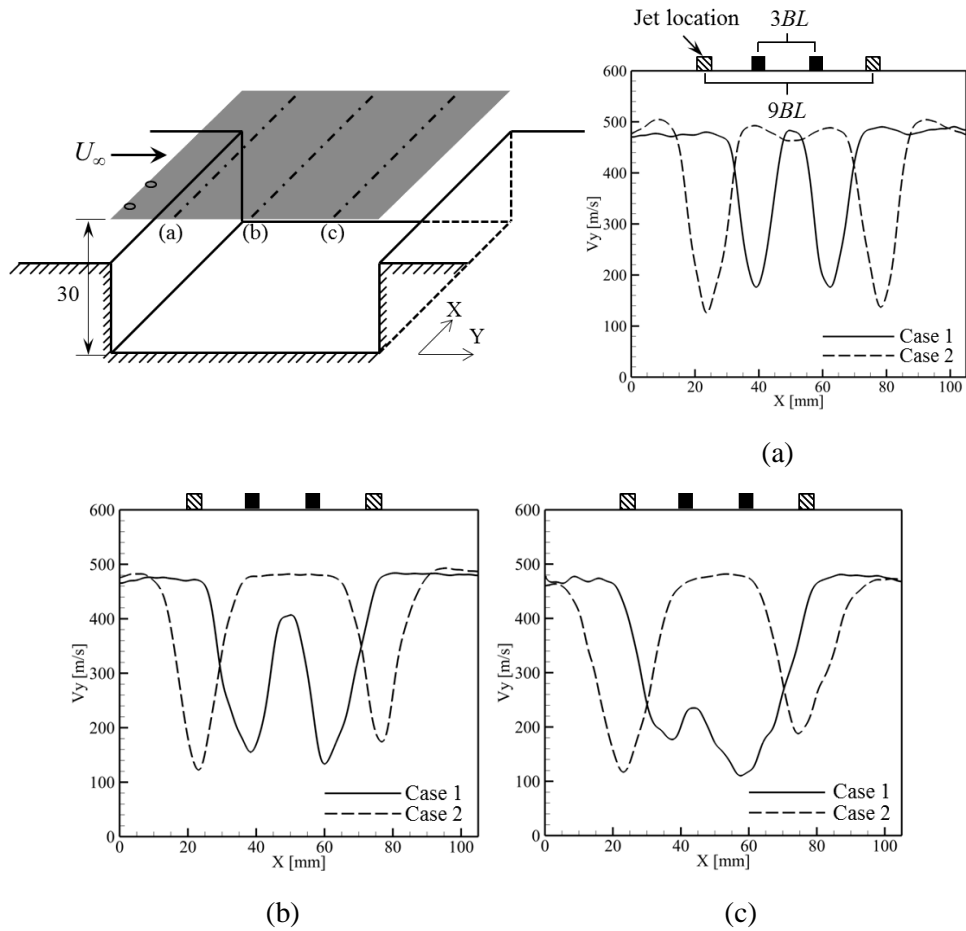


Figure 11: Velocity profile in the plane 30 mm above the cavity floor.
 (a) 80 mm, (b) 40 mm, and (c) 10 mm from the rear edge of the cavity.

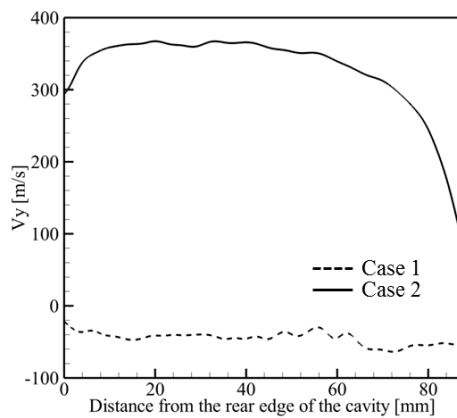


Figure 12: Velocity profile along the cavity centerline in the plane 20 mm above the cavity floor.

Table

Table 1: Averaged root-mean-square flow velocity along cavity centerline in the plane 10 mm above the cavity floor.

	Case 0	Case 1	Case 2
$V_{x\ rms}$	18.9	22.2	23.1
$V_{y\ rms}$	24.1	24.5	29.2